Journal of Materials Chemistry B

ROYAL SOCIETY OF CHEMISTRY

PAPER

View Article Online
View Journal | View Issue

Cite this: J. Mater. Chem. B, 2021, 9, 5150

A ratiometric near-infrared fluorescent probe based on a novel reactive cyanine platform for mitochondrial pH detection†

Shulin Wan,[a] Shuai Xia,[a] Jerry Medford,[a] Emma Durocher,[a] Tessa E. Steenwinkel,[b] Lexi Rule,[a] Yibin Zhang,[a] Rudy L. Luck,*[a] Thomas Werner*[b] and Haiying Liu*[a]

Received 25th March 2021,
Accepted 6th June 2021

DOI: 10.1039/d1tb00643f

rsc.li/materials-b

A near-infrared reactive cyanine platform (probe **A**) was prepared by condensation of 9-chloro-1,2,3,4-tetrahydro-10-methyl-acridinium iodide with Fisher's aldehyde. A near-infrared fluorescent probe (probe **B**) was prepared by modifying a reactive chlorine atom of probe **A** with *tert*-butyl(2-aminoethyl)carbamate through a substitution reaction. The deprotection of the Boc group of probe **B** was achieved under an acidic condition, affording an amine-functionalized cyanine dye (probe **C**). A near-infrared ratiometric fluorescent probe (probe **D**) for mitochondrial pH detection was synthesized by conjugating a FRET coumarin donor to a FRET cyanine acceptor (probe **C**) through an amide bond connection. Probe **A** shows low fluorescence of 2% due to an electron-withdrawing chlorine atom, while probes **B–D** display high fluorescence quantum yields of 60%, 32%, and 35% in aqueous solutions containing 10% ethanol, respectively. Probes **B–D** show strong fluorescence with push–pull molecular structures in neutral and basic pH conditions. However, protonation of the probe's second amine at the 9-position under acidic condition disrupts the push–pull feature of the probes, resulting in fluorescence quenching of the new cyanine fluorophores. The probes can selectively stain mitochondria, while probe **D** was employed to detect pH changes in HeLa cells and *Drosophila melanogaster* first-instar larvae.

Introduction

Cyanine dyes are a unique group of near-infrared fluorophores, consisting of pentamethine or heptamethine backbones with two nitrogen-containing heterocycles.[1–7] The U.S. Food and Drug Administration has approved indocyanine green for clinical applications due to its appealing near-infrared optical property.[4,8,9] Many fluorescent probes have been developed by modifying a central active chlorine atom of traditional cyanine dyes with amine-, thiol- and boron ester-functionalized compounds through substitution reactions for a variety of sensing and imaging applications.[1–5,7,10] Positively charged cyanine dyes have been used to specifically target mitochondria. However, due to the high-lying occupied molecular orbital (HOMO) energy levels of the cyanine dye, it is difficult to synthesize cyanine dyes with on–off switches. Recently, near-infrared hemicyanine dyes bearing spironolactone, spirolactam, and oxazolidine switches have also been developed for pH sensing and the detection of reactive nitrogen, oxygen, and sulfur species.[4,11–18] Most neutral fluorescent probes based on spirolactam switches have been used to detect pH changes in lysosomes,[12,14,15,19–25] while positively charged fluorescent probes with oxazolidine and spiropyran switches were employed to determine pH changes in mitochondria.[18,26] Despite significant progress in cyanine dye research, there are few reports on new cyanine platforms with reactive sites for on–off switchable probes. Therefore, it is very important to develop new near-infrared cyanine platforms with unique chemical structures and easy post-functionalization for sensing and imaging applications.

In this paper, we developed a novel near-infrared fluorescent cyanine platform (probe **A**) with a reactive chlorine atom by condensing 9-chloro-1,2,3,4-tetrahydro-10-methyl-acridinium iodide with Fisher's aldehyde (Chart 1). We further modified the reactive chlorine atom on probe **A** with *tert*-butyl(2-aminoethyl)carbamate by a substitution reaction, affording a secondary amine-functionalized pH sensitively "on–off" switchable cyanine dye (probe **B**). The Boc group in probe **B** was then removed, resulting in an amine-terminating cyanine dye (probe **C**). In order

[a] Department of Chemistry, Michigan Technological University, Houghton, MI 49931, USA. E-mail: hyliu@mtu.edu, rluck@mtu.edu
[b] Department of Biological Sciences, Michigan Technological University, Houghton, MI 49931, USA. E-mail: twerner@mtu.edu

† Electronic supplementary information (ESI) available: It includes NMR spectra of probes **A–D**, mass spectra of the probes in neutral and acidic conditions, calculations of the probe fluorescence quantum yields, pK_a values, the probes' reversible fluorescence responses to pH changes, and computational results. See DOI: 10.1039/d1tb00643f

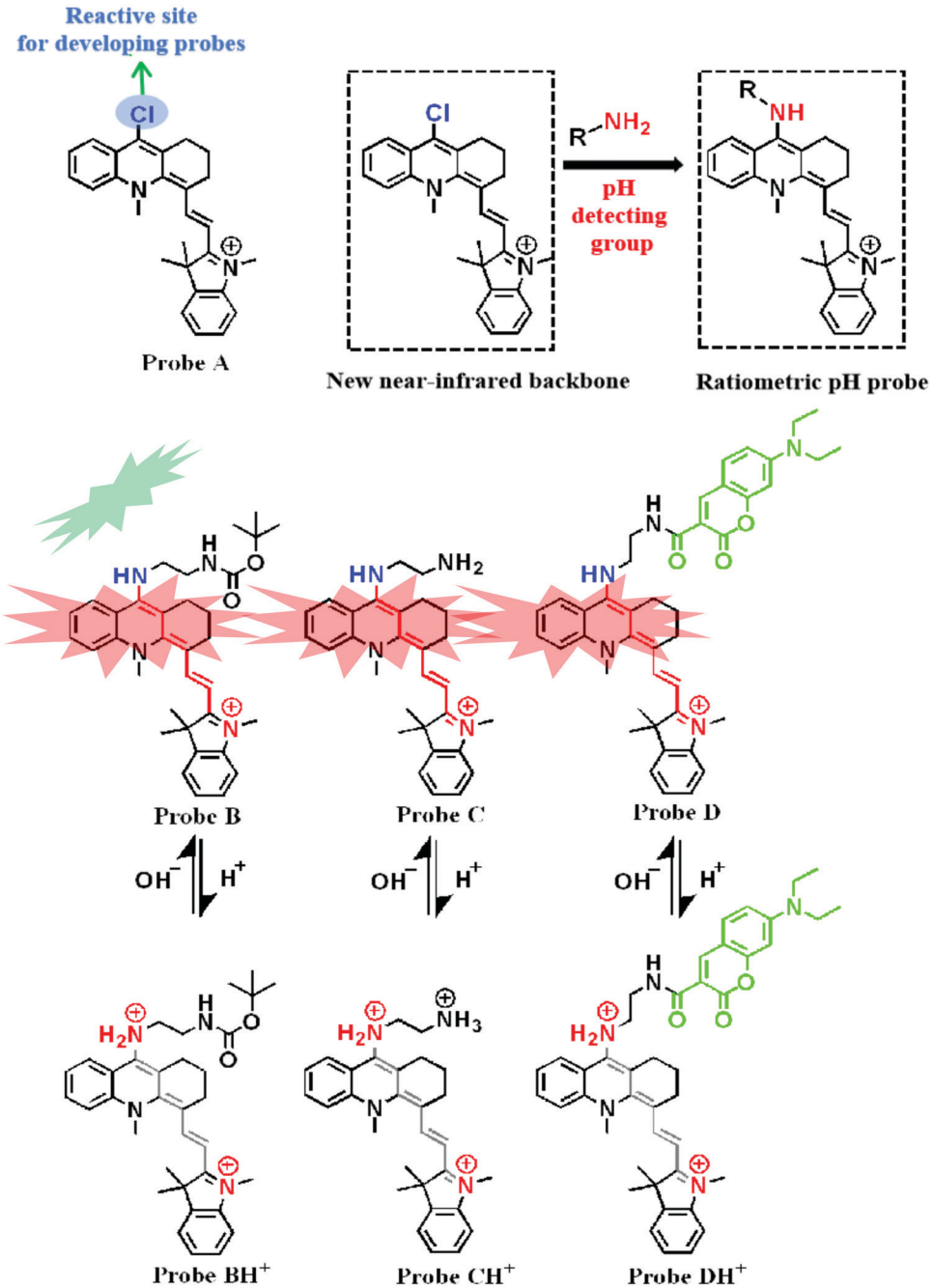

Chart 1 Reactive cyanine dye platform (probe **A**) and its derivatives (probes **B**, **C**, and **D**) for pH detection in mitochondria.

to achieve ratiometric imaging of pH changes, we introduced a coumarin moiety as a Förster Resonance Energy Transfer (FRET) donor to probe **C** through an amide bond connection to prepare a near-infrared cyanine dye, probe **D**.[27–30] FRET from a fluorophore donor to a fluorophore acceptor is often used to construct ratiometric fluorescent probes.[27,29–31] FRET efficiency depends significantly on the connection distance between the donor and acceptor and the overlap degree between the donor emission and acceptor absorption.[27,29–31] In probe **D**, the coumarin donor was connected to the cyanine acceptor through a very short two-methylene tethered spacer to achieve high efficiency of energy transfer from the donor to the acceptor since the acceptor absorption has significant overlap with the donor emission. Ratiometric fluorescent probes with self-calibration capabilities can effectively overcome systematic errors of intensity-based only fluorescent probes caused by excitation light fluctuations, probe concentration variations, and different cellular compartmental locations.[27,29] Probe **A** is insensitive to pH changes, while probes **C–D** show pH-sensitive responses (Chart 1), which are completely different from the acid-activated enhanced fluorescence of fluorescent probes based on spirolactam, spiropyran, and oxazolidine switches.[12,14,15,18–26] Gradual pH decreases lead to

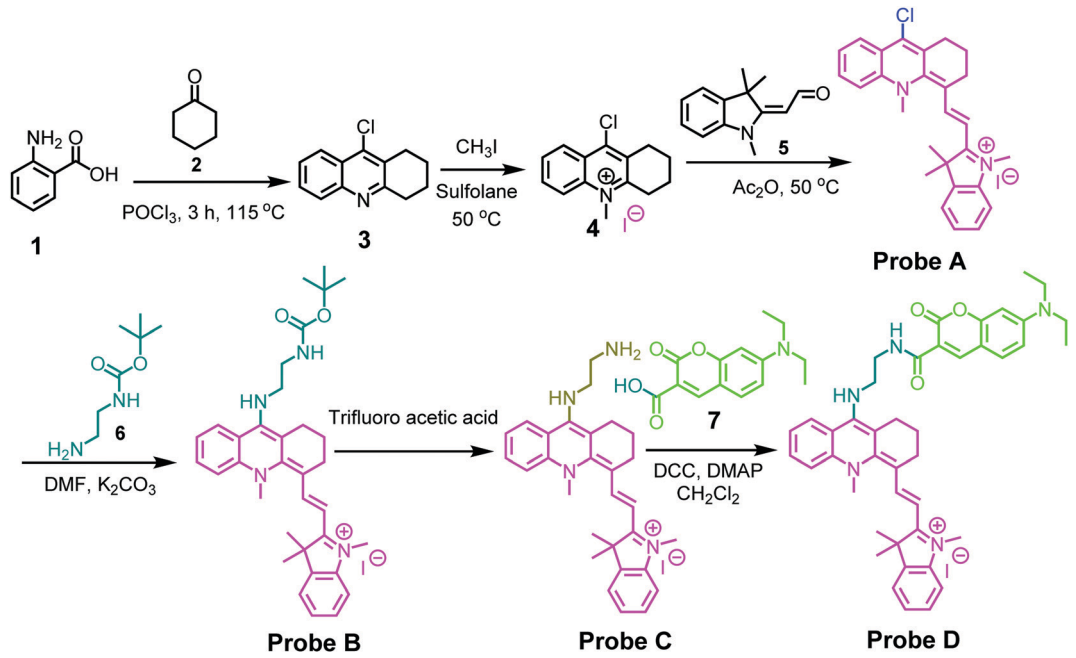

Scheme 1 Synthetic approach to prepare a near-infrared reactive cyanine dye backbone (probe **A**) and its derivatives (probes **B–D**).

fluorescence decreases of near-infrared fluorescence of probes **B–C**. Probe **D** shows ratiometric responses to pH decreases with fluorescence decreases of the cyanine acceptor and fluorescence increases of the coumarin donor. Ratiometric responses of probe **D** to pH arise from a high-efficiency energy transfer rate of 97.7% from the coumarin donor to the cyanine acceptor. The fluorescence decreases of the cyanine fluorophores arise from the disruption of push–pull molecular structures upon acidic-pH protonation of the secondary amine in the 9-position of the probes (Chart 1). The positively charged probes **A–D** can specifically target mitochondria through electrostatic interactions with the negatively charged mitochondrial matrix. Probe **D** shows sensitive fluorescence responses to pH changes in live cells and *Drosophila melanogaster* (*D. melanogaster*) first-instar larvae.

Materials and instruments

Details of regents and instruments are documented in the ESI.†

Synthesis of probe A

Fisher's aldehyde (**5**) (112 mg, 0.56 mmol) was added to 6 mL of acetic anhydride containing compound **4** (200 mg, 0.56 mmol).[12,23] The mixture was then stirred at 50 °C for 2 h, Scheme 1. The reaction mixture was evaporated under vacuum. The crude product was purified through column chromatography (packed with silica gel, particle size, 0.063–0.2 mm Merck) and eluted with a mixture of dichloromethane and MeOH at ratios from 100 : 1 to 30 : 1, yielding pure probe **A** in the form of blue crystals (233 mg with a reaction yield of 70%). ^{1}H NMR (400 MHz, $CDCl_3$) δ 8.31 (d, J = 8.6 Hz, 1H), 8.15 (d, J = 9.7 Hz, 1H), 7.97–7.86 (m, 1H), 7.60 (t, J = 7.7 Hz, 1H), 7.43 (d, J = 13.3 Hz, 1H), 7.32 (d, J = 7.2 Hz, 1H), 7.24 (d, J = 7.5 Hz, 1H), 7.11–7.03 (m, 1H), 6.98 (d, J = 7.5 Hz, 1H), 5.77 (d, J = 13.0 Hz, 1H), 4.48 (s, 3H), 3.53 (s, 3H), 2.95 (t, J = 5.8 Hz, 2H), 2.81 (t, J = 6.2 Hz, 2H), 1.97 (t, J = 6.0 Hz, 2H), 1.58 (s, 6H). ^{13}C NMR (101 MHz, $CDCl_3$) δ 174.39, 170.82, 158.19, 145.56, 141.27, 140.90, 133.95, 133.76, 128.55, 127.59, 125.65, 124.16, 123.91, 122.30, 120.10, 116.73, 110.99, 109.72, 104.94, 96.36, 49.19, 48.74, 47.93, 29.89, 28.98, 28.40, 28.14, 20.77. MS (ESI): calcd for $[C_{34}H_{43}N_4O_2]^+$ 415.1936, found 415.1927.

Synthesis of probe B

Probe **A** (200 mg, 0.48 mmol) was added to 6 mL dimethylformamide (DMF) containing boc-ethylenediamine (153 mg, 0.96 mmol). This mixture was stirred at 50 °C for 2 h, whereupon it was poured into 100 mL of dichloromethane in a separatory funnel and washed with 50 mL saturated saline solution three times. The organic layer was collected, dried with anhydrous Na_2SO_4, and condensed under reduced pressure. The residue was subjected to column chromatography (packed with silica gel, particle size, 0.063–0.2 mm Merck) and eluted with a mixture of dichloromethane and MeOH at ratios from 70 : 1 to 50 : 1, yielding the pure probe **B** in the form of red crystals (207 mg with a reaction yield of 80%). ^{1}H NMR (400 MHz, $CDCl_3$) δ 8.56 (d, J = 10.1 Hz, 1H), 7.85 (d, J = 4.2 Hz, 1H), 7.63–7.49 (m, 2H), 7.19 (dd, J = 17.5, 7.7 Hz, 2H), 6.99–6.85 (m, 2H), 6.77 (d, J = 8.3 Hz, 1H), 5.95 (s, 1H), 5.46 (d, J = 12.6 Hz, 1H), 4.16 (s, 3H), 4.10–4.02 (m, 2H), 3.72–3.61 (m, 2H), 3.27 (s, 3H), 2.94–2.83 (m, 2H), 2.76–2.66 (m, 2H), 1.99–1.86 (m, 2H), 1.54 (s, 6H), 1.37 (s, 9H). ^{13}C NMR (101 MHz, $CDCl_3$) δ 163.92, 158.02, 156.80, 153.62, 144.22, 141.09, 139.12, 136.26, 133.04, 128.27, 125.76, 121.90, 121.54, 118.86, 118.32, 118.05, 115.94, 107.49, 92.12, 79.97, 50.92, 46.70, 43.43, 40.89, 29.99, 29.71, 28.70, 26.83, 22.74. MS (ESI): calcd for $[C_{34}H_{43}N_4O_2]^+$ 539.3481, found 539.3364.

Synthesis of probe C

After a solution of probe **B** (200 mg, 0.37 mmol) in 6 mL dichloromethane was cooled by being surrounded by a mixture of ice and water, 6 mL of trifluoracetic acid (TFA) were added dropwise. The reaction mixture was stirred at room temperature for 6 h, and the solvent evaporated under reduced pressure. The crude product was subjected to column chromatography (packed with silica gel, particle size, 0.063–0.2 mm Merck) and eluted with a mixture of dichloromethane and MeOH at a ratio of 10 : 1, yielding probe **C** in the form of red crystals (146 mg with a reaction yield of 90%). ^{1}H NMR (400 MHz, $CDCl_3$) δ 8.49 (d, J = 9.0 Hz, 1H), 7.96 (s, 2H), 7.80 (s, 2H), 7.59–7.51 (m, 1H), 7.22–7.17 (t, 1H), 7.14 (d, J = 7.5 Hz, 1H), 6.95–6.84 (m, 2H), 6.74 (d, J = 7.2 Hz, 1H), 5.44 (d, J = 12.8 Hz, 1H), 5.26 (s, 1H), 4.13 (s, 3H), 3.43–3.48 (m, 2H), 3.24 (s, 3H), 2.86–2.78 (m, 2H), 2.68–2.66 (m, 2H), 1.93–1.84 (m, 2H), 1.51 (s, 6H), 1.39 (d, J = 7.0 Hz, 2H). ^{13}C NMR (101 MHz, $CDCl_3$) δ 163.79, 161.77, 161.43, 157.37, 153.60, 144.26, 140.85, 139.22, 136.40, 132.83, 128.24, 125.91, 125.37, 121.91, 121.32, 119.16, 118.67, 118.47, 117.97, 117.17, 115.55, 107.38, 92.27, 46.63, 42.99, 39.97, 29.85, 29.55, 22.61. MS (ESI): calcd for $[C_{29}H_{35}N_4]^+$ 439.2856, found 439.2843.

Synthesis of probe D

To activate the carboxylic acid group of 7-(diethylamino)-coumarin-3-carboxylic acid (7), BOP (301 mg, 0.68 mmol) and *N*,*N*-diisopropylethylamine (DIPEA) (176 mg, 1.36 mmol) were added into a solution of compound 7 (118 mg, 0.45 mmol) in 6 mL dichloromethane and then stirred at room temperature for 20 min. After probe **C** (197 mg, 0.45 mmol) was added to the reaction mixture, the mixture was stirred at room temperature for 6 h under a nitrogen atmosphere. The solvent was then removed by evaporation under vacuum, and the product was subjected to column chromatography (packed with silica gel, particle size, 0.063–0.2 mm Merck) and eluted with mixtures of dichloromethane and MeOH at ratios from 100 : 1 to 50 : 1, resulting in pure probe **D** in the form of a red solid (180 mg, 60% reaction yield). ^{1}H NMR (400 MHz, $CDCl_3$) δ 9.16–8.97 (m, 1H), 8.70 (d, J = 9.3 Hz, 1H), 8.59 (s, 1H), δ 7.81 (d, J = 5.6 Hz, 1H), 7.60 (s, 1H), 7.38 (d, J = 8.9 Hz, 1H), 7.23–7.09 (m, 2H), 6.95–6.83 (m, 2H), 6.74 (d, J = 8.0 Hz, 1H), 6.61 (dd, J = 8.9, 1.9 Hz, 1H), 6.41 (d, J = 1.9 Hz, 1H), 5.43 (d, J = 11.9 Hz, 1H), 4.13 (s, 3H), 3.68–3.58 (m, 2H), 3.46–3.34 (m, 4H), 3.24 (s, 3H), 3.13–3.03 (m, 2H), 2.99–2.92 (m, 2H), 2.74–2.64 (m, 2H), 1.96–1.87 (m, 2H), 1.52 (s, 6H), 1.27–1.09 (t, 6H). ^{13}C NMR (101 MHz, $CDCl_3$) δ 166.43, 164.31, 162.74, 157.99, 157.20, 153.29, 148.66, 144.21, 141.27, 139.36, 136.77, 133.13, 131.69, 128.14, 125.77, 124.68, 121.93, 121.52, 118.76, 118.67, 117.98, 115.92, 110.65, 108.57, 108.43, 107.45, 96.64, 92.20, 52.26, 47.32, 46.75, 45.46, 43.27, 40.72, 29.87, 29.53, 26.76, 26.33, 22.70, 12.72, 9.15. MS (ESI): calcd for $[C_{43}H_{48}N_5O_3]^+$ 682.3752, found 682.3731.

Fluorescence imaging of HeLa cells

The HeLa cell line was acquired from ATCC and cultured according to our previously reported procedures.[10,12,14–16,19,20,23,32–34] For colocalization experiments, the HeLa cells were incubated with 5 μM probe **A**, **B**, or **C** with commercially available mitochondria-targeting MitoView Blue (5 μM) for 15 minutes. In order to avoid fluorescence overlap between probe **D** and MitoView Blue, we incubated HeLa cells with probe **D** with a mitochondria-targeting near-infrared cyanine dye (IR-780) (5 μM) for the colocalization experiment. A 0.2% DMSO concentration was used during the cell incubation to facilitate the dye solubility in the cell culture medium. The fluorescence imaging was conducted after the cells were washed twice with the cell culture medium, and added with the cell culture medium. In order to detect intracellular pH changes in live cells, we incubated HeLa cells with 5 μM probe **D** in the cell culture medium for 15 minutes, washed with the medium twice, and then further incubated in different pH buffer solutions in the presence of 5 μg mL^{-1} nigericin, a K^+/H^+ ionophore for 20 minutes, to reach equilibrium between intracellular pH and extracelluar pH.[32–34] We conducted fluorescence imaging of HeLa with different intracellular pH values after the cells were rinsed twice with the medium. Fluorescence of Mito-Vew Blue was collected from 435 nm to 475 nm under excitation at 405 nm, while the fluorescence of probes **A**, **B**, and **C** were collected from 625 nm to 675 nm under 559 nm excitation. The fluorescence of the cyanine dye (IR-780) was collected from 750 nm to 800 nm at 635 nm excitation, while the fluorescence of probe **D** was collected from 475 nm to 525 nm (for the coumarin donor emission) and from 625 nm to 675 nm (for cyanine acceptor fluorescence) under 405 nm excitation. The fluorescence of probe **D** was also collected for acceptor fluorescence from 625 nm to 675 nm under 559 nm excitation.

Fluorescence imaging of *Drosophila melanogaster* larvae

In order to demonstrate the feasibility of probe **D** for an *in vivo* system, we submerged freshly hatched fruit fly larvae in three different pH buffer solutions containing 10 μM probe **D** and 0.5% DMSO for 2 h, respectively. Fluorescence imaging was conducted after the fruit fly larvae were washed three times with deionized water.

Results and discussion

Design and synthesis of the probes

We have developed a new cyanine-based fluorescence platform consisting of conjugated indole and acridine moieties to produce near-infrared pH-responsive probes. This platform has a long π-conjugation system and a reactive chlorine atom at the 9-position of acridine, which facilitates functionalization with amine- and thiol derivatives, resulting in probes that can be utilized for various sensing and imaging applications. The functionalization of this new platform with amine derivatives allows us to alter optical properties of the probes by modulating the electron-donating or electron-withdrawing status of the nitrogen atom at the 9-position varies upon pH changes.

We synthesized 9-chloro-1,2,3,4-tetrahydro-acridine (**3**) through condensation of anthranilic acid (**1**) and cyclohexanone (**2**) in fresh $POCl_3$ at high temperature[35–37] and then converted compound **3** to 9-chloro-1,2,3,4-tetrahydro-10-methyl-acridinium iodide (**4**)

by reacting compound **3** with iodomethane in sulfolane at 50 °C (Scheme 1). The near-infrared cyanine dye with a reactive chlorine atom (probe **A**) was prepared by a condensation reaction of Fisher's aldehyde (**5**) with compound **4**.[34] A subsequent substitution reaction of the reactive chlorine atom of probe **A** with an amine residue from *tert*-butyl(2-aminoethyl)carbamate (**6**) afforded a Boc-functionalized cyanine dye (probe **B**).[16] The deprotection of the Boc group of probe **B** with trifluoroacetic acid gave a primary amine-functionalized cyanine dye (probe **C**) (Scheme 1). In order to detect pH changes ratiometrically, we prepared a near-infrared fluorescent probe (**D**) by introducing a 7-(diethylamino)coumarin-3-carboxylic acid (**7**) as a FRET donor to a near-infrared FRET cyanine acceptor (probe **C**) through an amide connection (Scheme 1). The probes were characterized by ^{1}H NMR, ^{13}C NMR, and high-resolution mass spectrometry (Fig. S1–S14, ESI†).

Optical properties of probes A–D

We found that the optical properties of this novel fluorescent platform are highly dependent on the electron donating ability of the substituents attached at the 9-position of the acridine moiety. Probe **A** shows an absorption peak at 592 nm and an emission peak at 660 nm with a low fluorescence quantum yield of 2% and 0.53% in an aqueous solution containing 10% ethanol and 0.1% DMSO, respectively. The low fluorescence quantum yield was observed in the near-infrared cyanine dye (IR 780) with a fluorescence quantum yield of 7% in a pure ethanol solution. We used a substitution reaction to replace the chlorine atom in probe **A** with a nitrogen atom, affording probes **B**, **C**, and **D**, respectively. Probes **B**, **C**, and **D** possess high fluorescence quantum yields of 60%, 32%, and 35% in an aqueous solution containing 10% ethanol, respectively. Probes **B**, **C**, and **D** display reduced fluorescence quantum yields of 18.2%, 10%, and 5.2% in pH 7.0 buffer solution containing 0.1% DMSO (Table S1, ESI†). Fluorescence quenching of the probes in almost pure buffer solvents is due to the aggregation-induced quenching effect, especially for probe **D** with a more hydrophobic feature (Table S1, ESI†).

Based on the fluorescent quantum yields of probes **A**, **B**, and **C**, we conclude that an electron-withdrawing group at 9-position will quench the fluorophore, while a donating group at the 9-position will enhance the fluorescence intensity of the fluorophores (probes **B**, **C**, and **D**). The conclusion inspired us to introduce an amine as the pH-responsive group to the reaction site on the 9-position of the acridine moiety. The amine group at

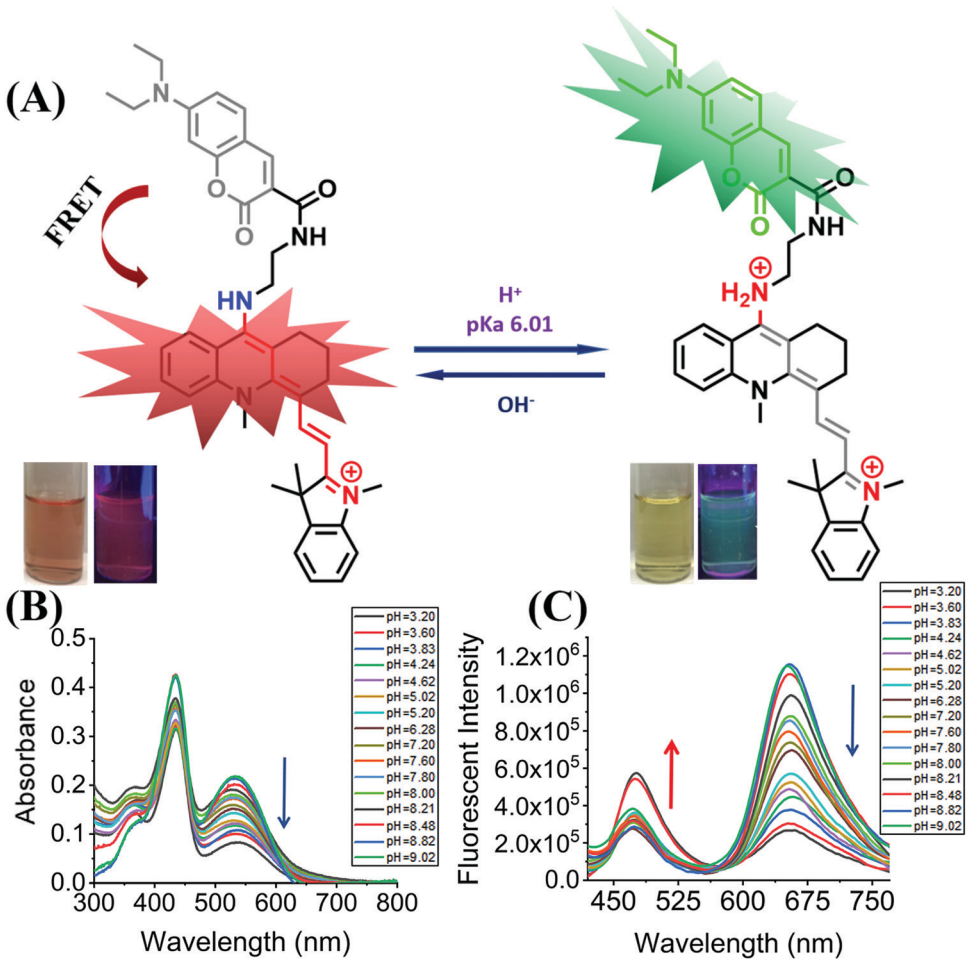

Fig. 1 (A) pH-dependent colors of buffer solutions containing probe **D** under visible light and UV light. Absorption (B) and fluorescence spectra (C) of probe **D** in different pH buffer solutions.

the 9-position is a strong electron-donating group under neutral conditions and can be changed into a strong electron-withdrawing group upon protonation with acid. This is expected to cause fluorescence quenching due to disruption of the push–pull molecular structure feature if the pH of the solution is decreased. Probe **A** shows insensitivity to pH changes as we expected (Fig. S15, ESI†). Probe **B** shows absorption and fluorescence peaks at 510 nm and 650 nm, respectively (Fig. S16, ESI†). Gradual decreases of the pH from 10.40 to 2.0 lead to decreases in both absorbance and fluorescence, which arise from protonation of the second amine of the cyanine dye at the 9-position (Fig. S16, ESI† and Chart 1). Probe **B** displays a pK_a value of 2.84 (Fig. S17, ESI†). Probe **C** displays similar responses to pH changes with a slightly lower pK_a value of 2.18 than probe **B** (Fig. S18 and S19, ESI†). Probe **D** shows two absorption peaks at 436 nm and 540 nm, responding to the absorption of the coumarin donor and cyanine acceptor (Fig. 1). Gradual pH decreases from 10.40 to 2.20 cause absorbance decreases of both the coumarin donor and the cyanine acceptor at 436 nm and 540 nm, respectively (Fig. 1B). It undergoes a drastic color change from pink to yellow when buffer pH decreases from 9.02 to 3.20 under daylight (Fig. 1A). However, probe **D** displays ratiometric fluorescence responses to pH changes from 7.0 to 3.0 with gradual fluorescence decreases of the cyanine acceptor and gradual fluorescence increases of the coumarin donor (Fig. 1C). The ratiometric responses of probe **D** arise from a high-efficiency energy transfer from the coumarin donor to the cyanine acceptor with an energy transfer rate of 97.7%. This is because the emission spectrum of the coumarin donor overlaps significantly with the absorption spectrum of the cyanine acceptor (Fig. S21, ESI†), which satisfies the requirement for fluorescence resonance energy transfer (FRET) from the donor to the acceptor. Solutions of probe **D** under UV light are red and green at pH values of 7.0 and 3.0, respectively (Fig. 1A). Probe **D** also displays a higher pK_a value of 6.01 (Fig. S21, ESI†) due to the bonding of the electron-withdrawing coumarin donor to the cyanine acceptor. Also, probes **B**, **C**, and **D** display reversible fluorescence responses to pH changes from 7.0 to 2.2 for probe **B** and **C**, from 9.01 to 3.2 for probe **D**, respectively (Fig. S22, ESI†). The stability of probes **B**, **C**, and **D** was also confirmed by high-resolution ESI mass spectroscopy under strongly acidic conditions (Fig. S23–S25, ESI†).

To explore the mechanism of the probe responses to acidic pH conditions, we investigated the ^{1}H NMR spectrum of probe **C** in the absence and presence of TFA in a $CDCl_3$ solution. As shown in Fig. S26 (ESI†), at acidic pH, peak a, assigned to the ethyl protons (adjacent to the amino group), shifts to peak a′. Peak b, assigned to the proton on the NH group, disappears after the addition of TFA, indicating that the NH group adjacent to the benzyl ring was protonated at acidic pH. Additionally, the benzyl protons c merged after treatment with TFA, indicating that the electronic conjugation within probe **C** changed under acidic conditions. We also observed a color change of probe **C** in the NMR tube from dark red to yellow after the acid treatment.

Under neutral and basic pH conditions, there are three amine groups with two electron-donating and electron-withdrawing features in probes **B–D**, which possesses push–pull features and results in strong fluorescence of the probes (Chart 2). However, protonation of the secondary amine at 9-position in acidic condition leads to fluorescence quenching because the systems possess two electron-withdrawing amine groups and one electron-donating amine group, disrupting push–pull features of the fluorophore. This unique structure of the probes allows for direct modulation of the probe absorption and fluorescence properties by altering the electron-donating/withdrawing nature of the central amine at 9-position through pH changes (Chart 2).

Probe selectivity and photostability

Probes **B**, **C** and **D** show good selectivity to pH over anions and cations such as Zn^{2+}, Ca^{2+}, Fe^{3+}, Hg^{2+}, Cd^{2+}, Ni^{2+}, and Mg^{2+}, NO_3^-, Cl^-, HCO_3^-, PO_4^{3-}, and CO_3^{2-} since the presence of 10 μM cations or anions does not cause any significant fluorescence changes (Fig. S27, ESI†).

Probes **A**, **B**, **C**, and **D** were excited continuously at 520 nm for 10 min intervals and the fluorescence intensity was measured

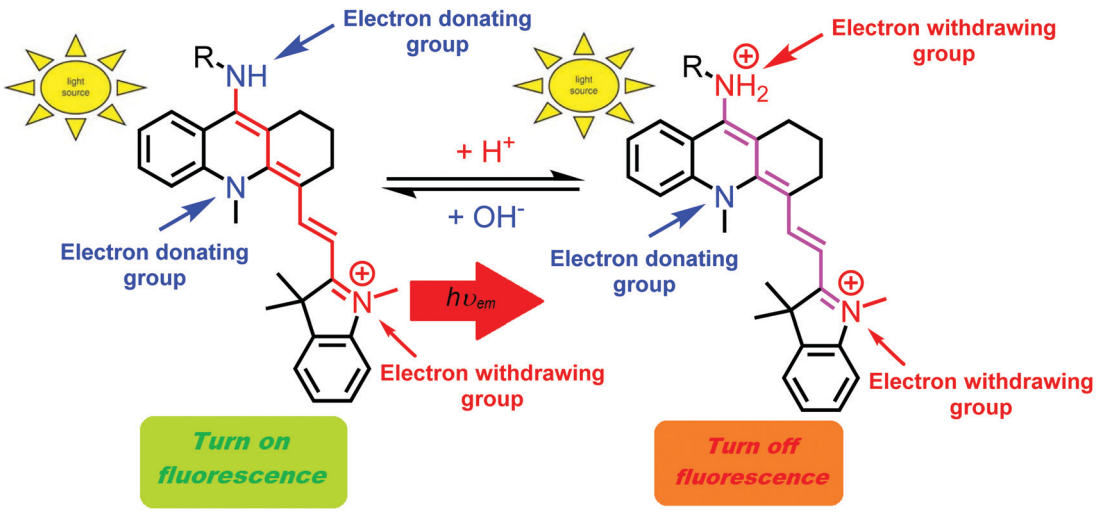

Chart 2 pH response mechanism of the probes based on the new cyanine platform.

every 10 min at pH 7.4. The result indicates that probes **A**, **B**, **C**, and **D** all displayed excellent photostability with less than 5% decrease only in fluorescence intensity under two-hour excitation at pH 7.4 (Fig. S28, ESI†).

Cytotoxicity of the probes

Standard MTT assays were carried out through 24 h incubation of HeLa cells with 1, 2, 5, 10, and 20 μM concentrations of probes **A**, **B**, **C**, or **D** (Fig. 2). The viability of the cells incubated with 10 μM probe **A**, **B**, **C**, and **D** are more than 85%, demonstrating that the probes own decent biocompatibility for biological studies. Probe **D** shows slightly lower cell viability than probes **B–D** because of its more hydrophobic feature with an additional coumarin donor (Fig. 2).

Theoretical results

Computational models of the probes and their expected protonated versions were calculated as outlined in the ESI.† The conformations obtained in a Polarizable Continuum Model (PCM) of water[38] contained dihedral angles between the indole and tetrahydro-acridine planes that varied slightly between the neutral and protonated versions of the probes with **A**, 41.31°; **B**, 44.32°; **BH$^+$**, 38.07°; **C**, 36.44°; **CH$^+$**, 39.06°; **D**, 39.30° and **DH$^+$**, 36.27°. However, while there were slight differences in this dihedral angle in probe **D**, there was a big difference in the location of the coumarin moieties resulting after protonation, as shown in Fig. 3.

Electronic transition calculations established that in probe **A**, a movement of electron density from the indole end of the molecule to the tetrahydro-acridine moiety occurs at 538 nm, as compared to the experimentally observed 600 nm (Fig. 4).

The higher energy transition was calculated to occur at 363 nm (345 nm expt. in water, see Fig. 1), which was in closer agreement and corresponded to an excited state with a higher electron density on the acridine moiety (Fig. S34, ESI†). For probe **A**, the calculated oscillating strengths of the two transitions matched the absorption profile for the spectrum obtained experimentally, as the UV transitions had calculated values of 0.3379 and 0.9728 for the observed transitions at 345 and 600 nm (Table S3, ESI† and Fig. 1). Probes **B** with attached carbamate and **C** with attached ethylenediamine and their protonated compounds did not differ substantially in their calculated transitions (Fig. 4), which may be due to a lack of orbital overlap and thus conjugation with these added substituents. Probe **D** was calculated to have a visible absorption at 494 nm (compared to 537 nm expt.), which was composed of a transition from the indole to the acridine moiety, as described earlier for Probes **A–C**. The higher energy transition calculated at 369 nm appears to be mainly based on an absorption located on the coumarin section of the probe (Table S13 and Fig. S49, ESI†). The profiles of the calculated absorptions for probe **D** matched those obtained experimentally (compare Fig. 1 and Fig. S49, ESI†) due to the contribution of transitions with high oscillating strength from excited states 5 and 6 (Table S13, ESI†). Upon protonation and formation of **DH$^+$**, the visible transition appears to be from the coumarin section of the molecule to a delocalized state consisting of orbitals localized on the acridine and indole moieties (Table S15, ESI†). The final calculated structure for probe **DH$^+$** appeared to have a sterically hindered geometry, but changing torsion angles and subsequent refining of the model resulted in a similar conformation. There are many ways to calculate pK_a values for molecules containing functional groups including amines.[39] For probes **B–D**, we utilized DFT together with the Solvation Model based on the Density (SMD) solvent model. This method resulted in substantial differences between the calculated and experimental data with an average ΔpK_a of 4.60 (Table 1). In a study on alcohols, phenols, and hydroperoxides, the addition of one water molecule directly to the site being protonated/deprotonated improved the accuracy of the calculation by as much as 3 pK_a units.[40] With probes **B–D**, the addition of one water molecule (Fig. S54, ESI†) reduced the average ΔpK_a from 4.60 to 0.64 (Table 1), which is comparable to the error range reported[40] with the inclusion of a cluster of three water molecules of 0.4 to 1.4 pK_a units. With the inclusion of one water molecule, we found the largest deviation for probe **C**, which contained two N atoms that could be protonated. The calculated values for the pK_a for the outer N atom on probe **C** at 7.58 deviated substantially from the experimentally obtained value of 2.18. The calculated value for the more centrally located N atom at 0.27 was closer to the experimental value, suggesting that

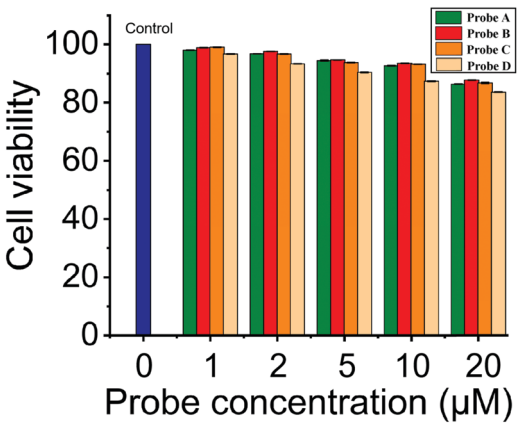

Fig. 2 MTT assays were used to evaluate the cytotoxicity of the probes through 24 h incubation of HeLa cells with different probe concentrations. The cell viability was determined by the absorbance obtained at 490 nm with three repeated measurements while cells without the probe were used as a control.

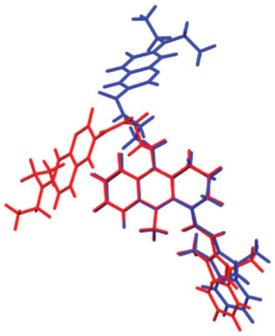

Fig. 3 Overlay of probe **D** (blue) and probe **DH$^+$** (red), showing the different positions of the coumarin moieties.

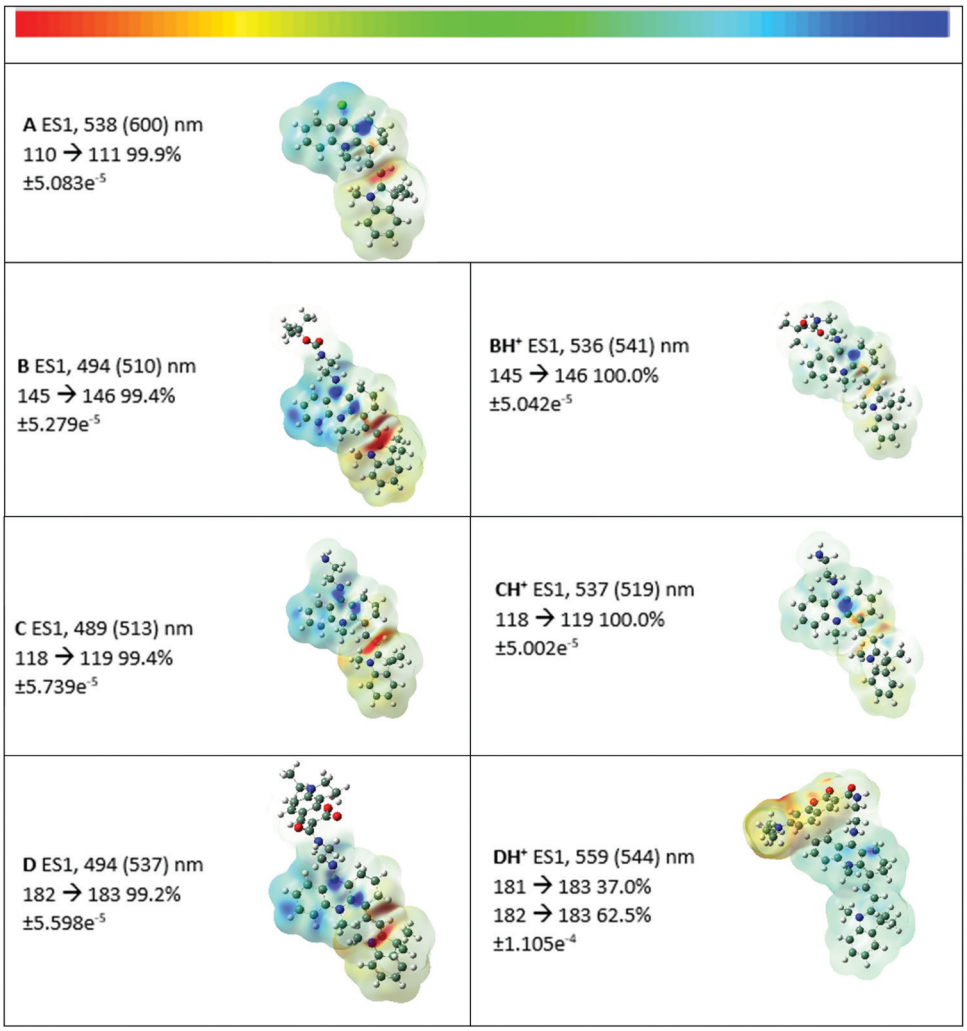

Fig. 4 Illustrations of the current density difference as isosurfaces of the probes and their protonated forms, as indicated for the excited states (ES) and the calculated (and experimental) wavelengths. The composition of specific ES, together with percentage contributions, are indicated. The numerical range values for the color scale illustrated at the top of the figure are also listed. Drawings of the numbered MOs are available in the ESI.†

Table 1 Experimental pK_a's and calculated pK_a's using the APFD/6-31+G(d) level of theory for the probes[a]

Probe	Experiment	SMD	ΔpK_a[b]	SMD + 1 water	ΔpK_a[b]
B	2.84	−1.19	−4.03	2.63	−0.21
C	2.18	−2.20	−4.38	0.27 (7.58)[c]	−1.61
D	6.01	0.62	−5.40	6.13	0.12

[a] Atomic positions and diagrams are in the ESI. [b] $\Delta pK_a = pK_{a,calculated} - pK_{a,experiment}$. [c] Added water located near the outer N atom in probe **C**.

this was the site of protonation/deprotonation. The results of these experiments suggest that a model consisting of SMD with one strategically placed water molecule would be a reasonable starting point for pK_a calculations of large molecules involving N atoms.

Cellular imaging of the probes

Mitochondria, double membrane-bound organelles that are the power producers within cells, convert nutrients and oxygen into adenosine triphosphate (ATP). They play very important roles in calcium homeostasis, regulation of the innate immunity, cellular signaling, and programmed cell death.[41] The mitochondrial functions also significantly depend on the intracellular pH. Therefore, it is important to accurately determine mitochondrial pH changes for an insightful understanding of mitochondrial physiology and pathology.

Since probes **A–D** are positively charged, we expected that they would specifically target mitochondria through electrostatic interactions as negative potentials are located within mitochondrial inner membranes.[32] In order to test this hypothesis, we conducted colocalization experiments by incubating HeLa cells with 5 μM probes **A–C** and 5 μM mitochondria-specific Mitoview Blue for 15 minutes, washing the cells with cell culture medium twice, and then adding cell culture medium to the cells for cellular imaging (Fig. S29–S31, ESI†). In order to avoid fluorescence interference of Mitoview Blue with coumarin donor fluorescence of probe **D**, we chose a mitochondria-specific cyanine dye IR-780 for the colocalization experiment by incubating HeLa cells with

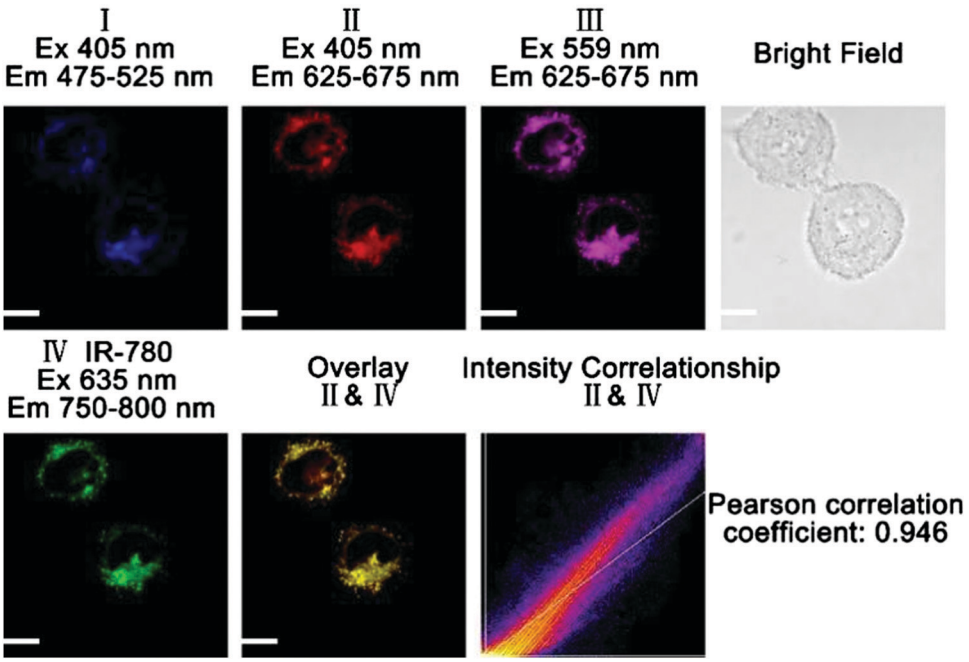

Fig. 5 Fluorescence images of HeLa cells incubated with 5 μM probe **D** and 5 μM cyanine dye (IR-780) for 15 minutes under excitation at 405 nm and 559 nm for probe **D** and under excitation at 635 nm for cyanine dye (IR-780). Scale bar: 20 μm. Fluorescence of probe **D** was collected from 475 to 525 nm for the donor fluorescence in channel I, and 625 nm to 675 nm for the acceptor fluorescence in channel II under the donor excitation at 405 nm. Fluorescence of probe **D** was also collected from 625 nm to 675 nm for the acceptor fluorescence under the acceptor excitation at 559 nm.

5 μM probe **D** and 5 μM cyanine dye IR-780 according to the same colocalization procedure used for probes **A–C** (Fig. 5). High Pearson correlation coefficients of 0.888, 0.857, and 0.901 were observed among probes **A**, **B**, and **C** incubated with Mitoview Blue

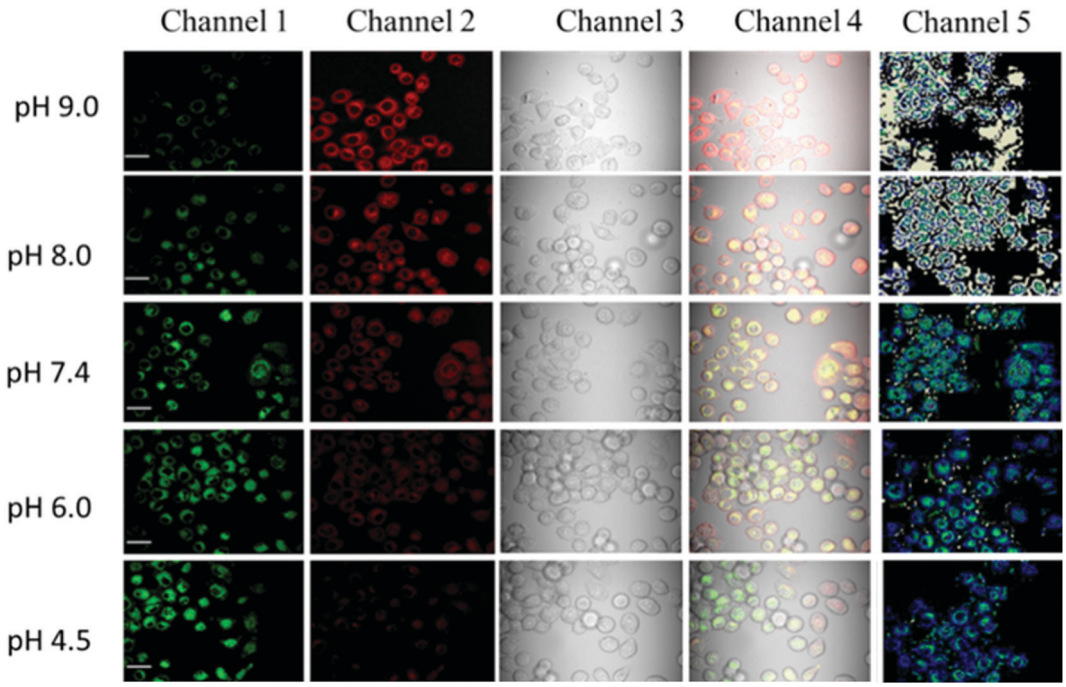

Fig. 6 Fluorescence images of HeLa cells incubated with 5 μM probe **D** under different cellular pH conditions with scale bars of 50 μm. HeLa cells were incubated with 5 μM probe **D** for 15 minutes, washed with cell culture medium twice, and then incubated in different pH buffers in the presence of 5 μg mL^{-1} nigericin, a K^+/H^+ ionophore for 20 minutes. Channel 1: the coumarin donor fluorescence collected from 475 to 525 nm at 405 nm excitation. Channel 2: the cyanine acceptor fluorescence collected from 600 to 700 nm at 405 nm excitation. Channel 3: bright-field. Channel 4: merged images of channels 1, 2, and 3. Channel 5: ratiometric images of channel 1 divided by channel 2, which were acquired with Image-Pro software.

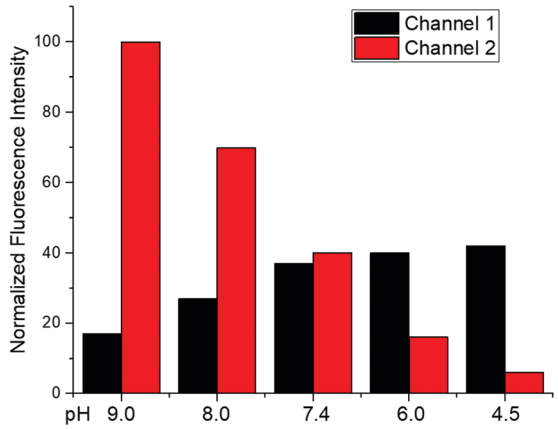

Fig. 7 Fluorescence intensity of the probe donor (channel 1) and acceptor (channel 2) in HeLa cells obtained from Fig. 6.

(Fig. 5–8), while the colocalization of probe **D** with the cyanine dye IR-780 resulted in a high Pearson correlation coefficient of 0.946. These results confirm that probes **A–D** do selectively stain mitochondria (Fig. S29–S31, ESI† and Fig. 5).

Intracellular pH imaging of probe D

We further used probe **D** to verify whether it can respond to pH changes in mitochondria as it possesses a higher pK_a value. We incubated probe **D** with HeLa cells in different pH buffer solutions in the presence of 5 μM nigericin, a K^+/H^+ ionophore, which is used to adjust intracellular pH to the buffer pH through pH equilibration.[10,12,14–16,19,20,23,32–34]

Probe **D** displays ratiometric fluorescent responses to intracellular pH changes with fluorescence decreases of the cyanine acceptor in channel 2 and fluorescence increases of the coumarin donor in channel 1 upon intracellular pH decreases from 9.0 to pH 4.5 (Fig. 6 and 7). The merged images (channel 4) of channels 1, 2, and 3 show drastic color changes from red to yellow and then to yellowish-green upon intracellular pH changes from 9.0 to 4.5. Furthermore, probe **D** also exhibits significant ratiometric color changes in channel 5 from bluish yellow to bluish green upon intracellular pH changes from 9.0 to 4.5 (Fig. 6).

Fluorescence visualization in *D. melanogaster* first-instar larvae

We chose probe **D** to test the feasibility of visualizing pH changes *in vivo*. We incubated first-instar *D. melanogaster* larvae with probe **D** in three different pH buffers for 2 h before conducting confocal fluorescence microscopy.[30,42] The larvae showed strong fluorescence of the cyanine acceptor and relatively weak fluorescence of the coumarin donor after incubation in a pH 7.0 buffer (Fig. 7). However, the larvae displayed weak fluorescence of the cyanine acceptor and relatively strong fluorescence of the coumarin donor after the larvae were incubated with probe **D** in a pH 5.0 buffer, which agrees with the ratiometric fluorescence responses of probe **D** to pH changes in buffer solutions (Fig. 1).

Conclusion

We have developed a new near-infrared cyanine dye with an easily substituted chlorine atom as well as three pH-sensitive

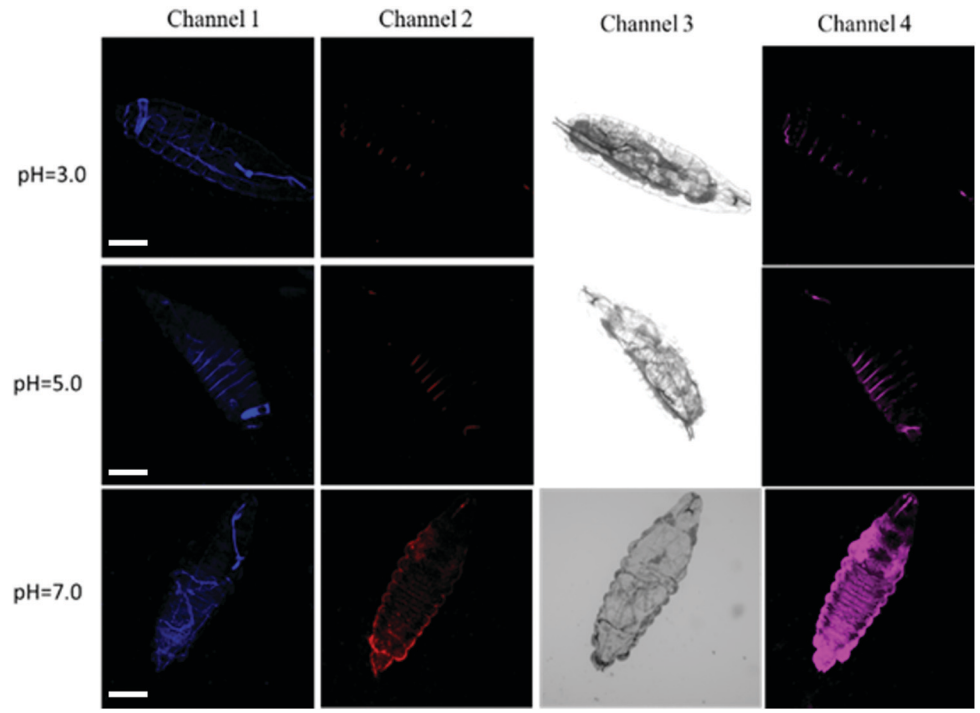

Fig. 8 Fluorescence images of *D. melanogaster* first-instar larvae incubated with fluorescent probe **D** in three different buffer solutions. Channel 1: the donor fluorescence collected from 475 to 525 nm at 405 nm excitation. Channel 2: the acceptor fluorescence collected from 600 to 700 nm at 405 nm excitation. Channel 3: bright-field. Channel 4: the acceptor fluorescence collected from 600 to 700 nm under 559 nm excitation. Scale bar: 200 μm.

near-infrared fluorescent probes with high fluorescence quantum yields. These three probes **B–D** were obtained by substituting the chlorine atom on probe **A** for a nitrogen atom bonded to three different substituents. Probes **B–C** show fluorescence decreases upon pH decreases, while probe **D** exhibits ratiometric fluorescence responses to pH decreases with fluorescence decreases of the cyanine acceptor and fluorescence increases of the coumarin donor. We have further demonstrated that probe **D** can be used to ratiometrically visualize pH changes in HeLa cells and *D. melanogaster* first-instar larvae.

Conflicts of interest

There are no conflicts to declare.

Acknowledgements

We greatly appreciate financial support for this research work by the National Institute of General Medical Sciences of the National Institutes of Health under Award Numbers R15GM114751 and 2R15GM114751-02 (to H. Y. Liu). The calculations of the fluorescent probe were conducted by using a high-performance computing infrastructure at Michigan Technological University.

References

1 J. L. Bricks, A. D. Kachkovskii, Y. L. Slominskii, A. O. Gerasov and S. V. Popov, *Dyes Pigm.*, 2015, **121**, 238–255.
2 A. P. Gorka, R. R. Nani and M. J. Schnermann, *Org. Biomol. Chem.*, 2015, **13**, 7584–7598.
3 H. A. Shindy, *Mini-Rev. Org. Chem.*, 2012, **9**, 352–360.
4 W. Sun, S. G. Guo, C. Hu, J. L. Fan and X. J. Peng, *Chem. Rev.*, 2016, **116**, 7768–7817.
5 L. Yuan, W. Y. Lin, K. B. Zheng, L. W. He and W. M. Huang, *Chem. Soc. Rev.*, 2013, **42**, 622–661.
6 Y. Li, Y. M. Zhou, X. L. Yue and Z. F. Dai, *Adv. Healthcare Mater.*, 2020, **9**, 2001327.
7 Z. Q. Guo, S. Park, J. Yoon and I. Shin, *Chem. Soc. Rev.*, 2014, **43**, 16–29.
8 R. Cadillo-Chavez, *Arch. Esp. Urol.*, 2019, **72**, 759–764.
9 A. Kumari and S. Gupta, *J. Biophotonics*, 2019, **12**, 1–7.
10 M. X. Fang, S. Xia, J. H. Bi, T. P. Wigstrom, L. Valenzano, J. B. Wang, W. Mazi, M. Tanasova, F. T. Luo and H. Y. Liu, *Chem. Commun.*, 2018, **54**, 1133–1136.
11 H. X. Li, H. Dong, M. M. Yu, C. X. Liu, Z. X. Li, L. H. Wei, L. D. Sun and H. Y. Zhang, *Anal. Chem.*, 2017, **89**, 8863–8869.
12 W. Mazi, R. Adhikari, Y. B. Zhang, S. Xia, M. X. Fang, R. L. Luck, M. Tajiri, A. Tiwari, M. Tanasova and H. Y. Liu, *Methods*, 2019, **168**, 40–50.
13 Y. X. Shi, X. C. Meng, H. R. Yang, L. N. Song, S. J. Liu, A. Q. Xu, Z. J. Chen, W. Huang and Q. Zhao, *J. Mater. Chem. B*, 2019, **7**, 3569–3575.
14 S. Xia, M. X. Fang, J. B. Wang, J. H. Bi, W. Mazi, Y. B. Zhang, R. L. Luck and H. Y. Liu, *Sens. Actuators, B*, 2019, **294**, 1–13.
15 S. Xia, J. B. Wang, J. H. Bi, X. Wang, M. X. Fang, T. Phillips, A. May, N. Conner, M. Tanasova, F. T. Luo and H. Y. Liu, *Sens. Actuators, B*, 2018, **265**, 699–708.
16 Y. B. Zhang, J. H. Bi, S. Xia, W. Mazi, S. L. Wan, L. Mikesell, R. L. Luck and H. Y. Liu, *Molecules*, 2018, **23**, 2679.
17 H. A. Shindy, *Dyes Pigm.*, 2017, **145**, 505–513.
18 W. Mazi, Y. N. Yan, Y. B. Zhang, S. Xia, S. L. Wan, M. Tajiri, R. L. Luck and H. Y. Liu, *J. Mater. Chem. B*, 2021, **9**, 857–863.
19 J. B. Wang, S. Xia, J. H. Bi, Y. B. Zhang, M. X. Fang, R. L. Luck, Y. B. Zeng, T. H. Chen, H. M. Lee and H. Y. Liu, *J. Mater. Chem. B*, 2019, **7**, 198–209.
20 M. X. Fang, R. Adhikari, J. H. Bi, W. Mazi, N. Dorh, J. B. Wang, N. Conner, J. Ainsley, T. G. Karabencheva-Christova, F. T. Luo, A. Tiwari and H. Y. Liu, *J. Mater. Chem. B*, 2017, **5**, 9579–9590.
21 T. H. Chen, S. W. Zhang, M. Jaishi, R. Adhikari, J. H. Bi, M. X. Fang, S. Xia, Y. B. Zhang, R. L. Luck, R. Pati, H. M. Lee, F. T. Luo, A. Tiwari and H. Y. Liu, *ACS Appl. Bio Mater.*, 2018, **1**, 549–560.
22 Y. B. Zhang, S. Xia, M. X. Fang, W. Mazi, Y. B. Zeng, T. Johnston, A. Pap, R. L. Luck and H. Y. Liu, *Chem. Commun.*, 2018, **54**, 7625–7628.
23 J. B. Wang, S. Xia, J. H. Bi, M. X. Fang, W. F. Mazi, Y. B. Zhang, N. Conner, F. T. Luo, H. P. Lu and H. Y. Liu, *Bioconjugate Chem.*, 2018, **29**, 1406–1418.
24 S. W. Zhang, T. H. Chen, H. M. Lee, J. H. Bi, A. Ghosh, M. X. Fang, Z. C. Qian, F. Xie, J. Ainsley, C. Christov, F. T. Luo, F. Zhao and H. Y. Liu, *ACS Sens.*, 2017, **2**, 924–931.
25 G. K. Vegesna, J. Janjanam, J. H. Bi, F. T. Luo, J. T. Zhang, C. Olds, A. Tiwari and H. Y. Liu, *J. Mater. Chem. B*, 2014, **2**, 4500–4508.
26 Y. B. Zhang, S. Xia, L. Mikesell, N. Whisman, M. X. Fang, T. E. Steenwinkel, K. Chen, R. L. Luck, T. Werner and H. Y. Liu, *ACS Appl. Bio Mater.*, 2019, **2**, 4986–4997.
27 L. L. Wu, C. S. Huang, B. Emery, A. C. Sedgwick, S. D. Bull, X. P. He, H. Tian, J. Yoon, J. L. Sessler and T. D. James, *Chem. Soc. Rev.*, 2020, **49**, 5110–5139.
28 R. J. Gui, H. Jin, X. N. Bu, Y. X. Fu, Z. H. Wang and Q. Y. Liu, *Coord. Chem. Rev.*, 2019, **383**, 82–103.
29 L. Yuan, W. Y. Lin, K. B. Zheng and S. S. Zhu, *Acc. Chem. Res.*, 2013, **46**, 1462–1473.
30 S. Xia, Y. B. Zhang, M. X. Fang, L. Mikesell, T. E. Steenwinkel, S. L. Wan, T. Phillips, R. L. Luck, T. Werner and H. Y. Liu, *ChemBioChem*, 2019, **20**, 1986–1994.
31 X. J. Zhang, Y. Hu, X. T. Yang, Y. Y. Tang, S. Y. Han, A. Kang, H. S. Deng, Y. M. Chi, D. Zhu and Y. Lu, *Biosens. Bioelectron.*, 2019, **138**, 111314.
32 S. A. Xia, J. B. Wang, Y. B. Zhang, N. Whisman, J. H. Bi, T. E. Steenwinkel, S. L. Wan, J. Medford, M. Tajiri, R. L. Luck, T. Werner and H. Y. Liu, *J. Mater. Chem. B*, 2020, **8**, 1603–1615.
33 J. T. Zhang, M. Yang, C. Li, N. Dorh, F. Xie, F. T. Luo, A. Tiwari and H. Y. Liu, *J. Mater. Chem. B*, 2015, **3**, 2173–2184.
34 J. T. Zhang, M. Yang, W. F. Mazi, K. Adhikari, M. X. Fang, F. Xie, L. Valenzano, A. Tiwari, F. T. Luo and H. Y. Liu, *ACS Sens.*, 2016, **1**, 158–165.

35 M. Scipioni, G. Kay, I. L. Megson and P. K. T. Lin, *MedChemComm*, 2019, **10**, 764–777.
36 X. J. Cheng, J. X. Gu, Y. P. Pang, J. Liu, T. Xu, X. R. Li, Y. Z. Hua, K. A. Newell, X. F. Huang, Y. H. Yu and Y. Liu, *ACS Chem. Neurosci.*, 2019, **10**, 3500–3509.
37 M. Scheiner, D. Dolles, S. Gunesch, M. Hoffmann, M. Nabissi, O. Marinelli, M. Naldi, M. Bartolin, S. Petralla, E. Poeta, B. Monti, C. Falkeis, M. Vieth, H. Hubner, P. Gmeiner, R. Maitra, T. Maurice and M. Decker, *J. Med. Chem.*, 2019, **62**, 9078–9102.
38 G. Scalmani and M. J. Frisch, *J. Chem. Phys.*, 2010, **132**, 114110.
39 P. Lian, R. C. Johnston, J. M. Parks and J. C. Smith, *J. Phys. Chem. A*, 2018, **122**, 4366–4374.
40 B. Thapa and H. B. Schlegel, *J. Phys. Chem. A*, 2017, **121**, 4698–4706.
41 S. W. G. Tait and D. R. Green, *J. Cell Sci.*, 2012, **125**, 807–815.
42 Y. B. Zhang, Y. N. Yan, S. Xia, S. L. Wan, T. E. Steenwinkel, J. Medford, E. Durocher, R. L. Luck, T. Werner and H. Y. Liu, *ACS Appl. Mater. Interfaces*, 2020, **12**, 20172–20179.